CHALMERS
UNIVERSITY OF TECHNOLOGY

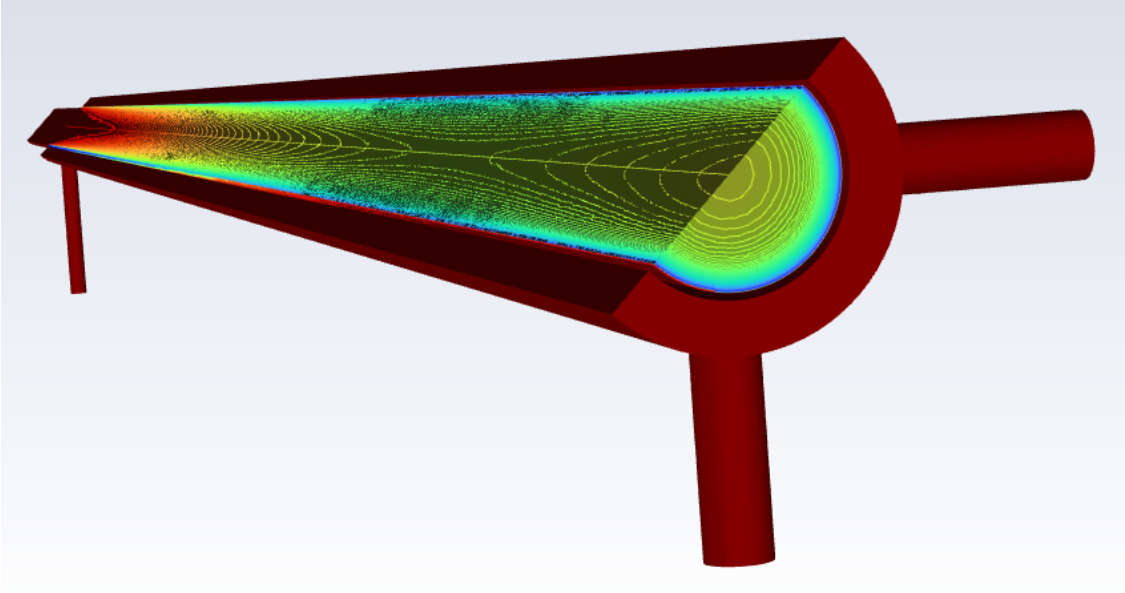

Numerical Study of Condensation and Conjugated Heat Transfer from Flow in a Heat Exchanger

Master's thesis in Applied Mechanics

Ehsan Peyvandi

DEPARTMENT OF MECHANICS AND MARITIME SCIENCES

CHALMERS UNIVERSITY OF TECHNOLOGY
Gothenburg, Sweden 2023
www.chalmers.se

Master's thesis 2023

Numerical Study of Condensation and Conjugated Heat Transfer from Flow in a Heat Exchanger

EHSAN PEYVANDI

CHALMERS
UNIVERSITY OF TECHNOLOGY

Department of Mechanics and Maritime Sciences
Division of Fluid Dynamics
Chalmers University of Technology
Gothenburg, Sweden 2023

Numerical Study of Condensation and Conjugated Heat Transfer from Flow in a Heat Exchanger
EHSAN PEYVANDI

Supervisor: Jonas Bredberg, PhD., Technical Account Manager, EDR&Medeso
Supervisor: Klas Johansson, PhD., Technical Business Development, EDR&Medeso
Supervisor: Fredrik Strömer, CFD Engineer, Alfa-Laval
Examiner: Srdjan Sasic, Professor, Department of Mechanics and Maritime Sciences, Chalmers University of Technology

Master's Thesis 2023
Department of Mechanics and Maritime Sciences
Chalmers University of Technology
SE-412 96 Gothenburg
Telephone +46 31 772 1000

Cover:
The image shows Mass transfer intensity constructed in Ansys Fluent where the blue and red color represents for maximum and zero mass transfer rate respectively

Printed by Chalmers Reproservice
Gothenburg, Sweden 2023

Numerical Study of Condensation and Conjugated Heat Transfer from Flow in a Heat Exchanger
EHSAN PEYVANDI
Department of Mechanics and Maritime Sciences
Chalmers University of Technology

Abstract

There are many industrial and nonindustrial fields where Plate heat exchangers, PHE, are utilized for their efficient heat transfer ability. Some fields in which PHEs are commonly used include HVAC (Heating, Ventilation, and Air Conditioning), Power Generation, and Refrigeration. The compact size, high heat transfer efficiency, ease of maintenance, and cleaning make them a popular option across various sectors. Hence, it is essential to study and understand the flow and heat transfer in plate heat exchangers to optimize the usage of these systems.

Alfa Laval develops (design, analyze, and manufacture) a wide range of heat exchangers, including gasketed, brazed, and welded plate models. This Master's thesis concentrated on investigating and laying the groundwork for conducting Computational Fluid Dynamics (CFD) simulations to study heat transfer during the phase change (condensation) process on the primary side, involving the full condensation of propane as it transitions from a gaseous to a liquid state.

The procedure followed in this thesis is as follows: Initially, a Pipe flow, as a first test case, is simulated to gain an understanding of the various parameters involved in Computational fluid dynamics (CFD) analysis. Then, as a second test case, to develop and validate a multiphase flow modeling where a full condensation of the gaseous phase occurs, the Kuhn (1995) [12] experiment is adopted.

The numerical simulation models were created using Ansys Discovery Modeling. Subsequently, the meshing and simulations were carried out using Ansys- Meshing and Fluent (2023R1). The hydrodynamics of the two-phase flow have been solved using both the Mixture- and Volume of Fluid (VoF) methods separately. Mass and heat transfer resulting from phase change (condensation) were handled through the Lee condensation model.

Keywords: CFD (Computational Fluid Dynamics), Multiphase Flow, Plate Heat Exchanger, Condensation, Simulation, Ansys- Meshing/Discovery/Fluent, Mixture- and Volume of Fluid (VoF) Multiphase Model.

Acknowledgements

I want to take the opportunity to acknowledge those who have helped me during my journey at Chalmers. First, I would like to thank the people at EDRMedeso, especially my supervisors Jonas Bredberg and Klas Johansson, for their constant support throughout the project. From Alfa-Laval, I would like to express my sincere gratitude to Fredrik Strömer for giving me this fantastic opportunity to participate in this challenging project. I would also like to thank Prof. Srdjan Sasic for being the examiner for this thesis work.

Lastly, I want to express my deepest gratitude to Eva Öresjö and Sverker Stomrud for their endless support and encouragement and for being an inspiration in all aspects of life. And my loving family, which I will always be thankful to have you in my life.

Ehsan Peyvandi, Gothenburg, May 2023

List of Acronyms

Below is the list of acronyms that have been used throughout this thesis listed in alphabetical order:

CFD	Computational Fluid Dynamics
HTC	Heat transfer coefficient
HVAC	Heating, Ventilation and Air Conditioning
RANS	Reynolds Averaged Navier-Stokes
SST	Shear Stress Transport
VoF	Volume of Fluid

Nomenclature

Below is the nomenclature of Latin and Greek symbols that have been used throughout this thesis.

Latin Symbols

A	Area, m^2
f_D	Friction factor, -
D	Diameter, m
C_p	Specific heat capacity, $J/(kg.K)$
F	Force, N
g	gravitation, m/s^2
h	Heat transfer coefficient, $W/(m^2.K)$
Q	Heat transfer, W
k	Turbulent kinetic energy, m^2/s^2
k	Thermal conductivity, W/(m.K)
L	Length, m
m	Mass, kg
$\dot{m}$	Mass flow rate, kg/s
P	Pressure, Pa
Re	Reynold's number, -
t	Time, s
T	Temperature, K
T_{sat}	Saturation temperature, K
T_l	Liquid temperature, K
T_v	Vapor temperature, K
T_i	Interfacial temperature, K
V	Velocity, m/s

y^+	Dimensionless wall distance

Greek Symbols

α	Volume fraction, -
ϵ	Turbulent dissipation rate, m^2/s^3
μ	Dynamic viscosity, $kg/(m.s)$
ν	Kinematic viscosity, m^2/s
ρ	Density, kg/m^3
∇	Gradient operator, -
ω	Turbulent dissipation rate, $1/s$
τ_w	Wall shear stress, Pa

Contents

1
Introduction

In this chapter, the motivation and the purpose for the current work will be presented. The outlines of the approach and strategy are described through different test cases, and the limitation of this thesis project is addressed.

1.1 Background

As global energy consumption continues to rise, the need to improve the efficiency of thermodynamic systems like Plate heat exchangers, PHE, is more than ever. PHE has widely been used in many industrial and non-industrial applications for both cooling and heating processes e.g., space heating, air conditioning, and refrigeration.

PHE is a type of heat exchanger in which heat is transferred between fluids, usually through a metal plate with high thermal conductivity [19]. PHEs are characterized by providing a large amount of heat transfer area in a relatively compact volume, making them a favored choice over traditional shell-and-tube heat exchangers. Moreover, it can easily be modified depending on heat transfer requirements by adding or removing plates to/from the stock.

There are several factors that affect the efficiency of transferring heat from one medium to the other, and the most important is the design of the metal plate that governs the channel. Cooling fins can be added and should be designed in such a way that the growth of boundary layers is prevented, leading to maximum turbulence as possible. Furthermore, the fluid channel's design should aim for uniform flow distribution to achieve the highest possible energy efficiency[14].

As PHEs have a significant role in various processes, it is of great importance that they operate at the highest efficiency to save energy. In order to optimize the capacity of PHE, it is crucial to understand how heat is transferred between the fluids during operation. Despite experimental studies being a trustworthy method, local flow phenomena still need to be studied. Therefore, carrying out a fast and robust numerical simulation to investigate the heat transfer characteristics inside the PHE is of great benefit.

Figure 1.1 (a) shows a schematic picture of the flow in a condenser design where the refrigerant enters at the top left of the heat exchanger as hot gas and starts to condense on the surface of the channels until fully condensed. Figure 1.1 (b) shows

the corrugated plates which are vacuum brazed together. The brazing process forms two channels for the participating media, generally flowing in opposite directions.

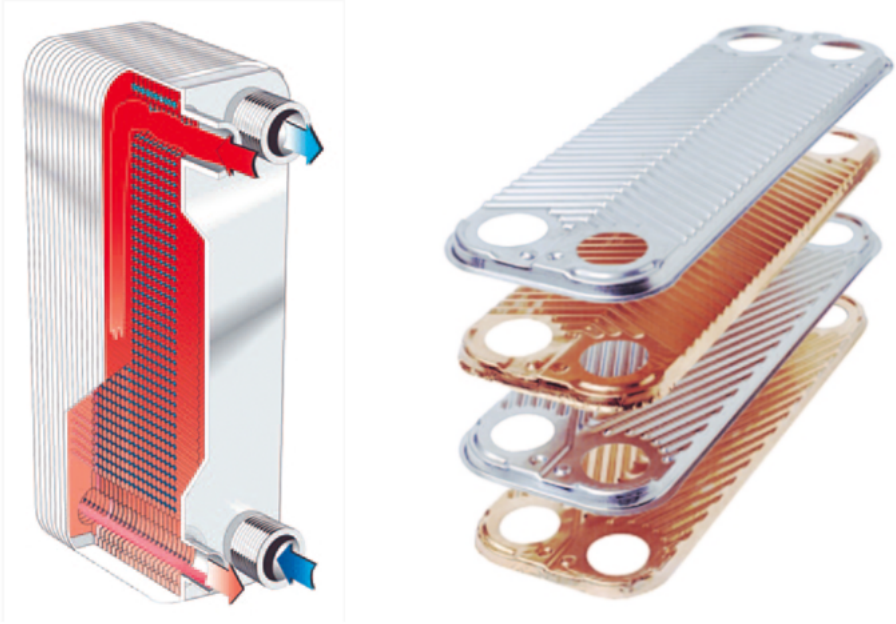

Figure 1.1: A schematic picture of a typical Brazed plate heat exchanger for condensation (Adopted from [13])

1.2 Purpose

As proposed by Alfa-Laval, the primary purpose of this thesis project is to develop a CFD multiphase model for conjugated heat transfer, including condensation, in a Plate heat exchanger that faithfully represents the laboratory test.

1.3 Methods

In order to fulfill the purpose of this thesis work, CFD (Computational fluid dynamics) with the FVM (Finite Volume Method) implemented in Ansys Fluent has been utilized. The task at hand has been conducted stepwise by considering first a simple pipe flow as an initial test case. Simulations on the pipe have been performed to get familiar with the different features of the software and to facilitate a mesh independency study. Additionally, *Kuhn's Experimentally Investigation of Heat Transfer from Condensing Steam-Gas Mixture Inside a Vertical Tube (1995)* [12] has been adopted as the second test case. The Mixture- and Volume of Fluid (VoF) multiphase model governs the hydrodynamics of the two-phase flow, separately, along with the Lee's evaporation-condensation model, to tackle the phase change (condensation) phenomena.

1.4 Limitations

Due to the complexities of multiphase modeling and time limitations, the scope of the thesis is limited to developing the foundations required for simulating the complete model of the Plate heat exchanger. Another limitation, as stated above, is that the simulation tools are limited to Ansys/Fluent and the functionality provided by the software.

2
Literature Review

2.1 Experimental studies

Many researchers have conducted experimental studies of condensation. Siddique (1993) [21] performed an experimental study of condensation in vertical tubes. The aim was to determine the effects of non-condensable gases (air and helium) on in-tube steam condensation under forced convection conditions. The condenser tube used had an outer- and inner diameter of 50.8 and 46 mm, respectively, where the condensation occurs at the inner surface with an effective length of 2.54 m. A 62.7 mm inner diameter concentric jacket pipe surrounded the test condenser. They concluded that the local heat transfer coefficient depends on the mixture flow Reynolds number, and they found out that helium has a more inhabiting effect on the heat transfer for the same mass fraction of non-condensable gas, compared with air. However, the air was found to be inhabiting for the same molar ratio.

Hisham A. Hasanein (1994) [11] performed an experimental and theoretical condensation investigation on the same test section dimension as Siddique. For a turbulent mixture flow ($Re > 5000$), the condensate film thermal resistance is reported to be significant. In contrast, the thermal resistance of the steam/non-condensable is more pronounced for laminar forced convection. Other researchers like Al Shammari (2004) [20] and Tanrikut (2007) [1] have also performed the same experiment but with different geometry, where the primary purpose was to see the effect of non-condensable gases on condensation rate.

Ambrosini et. al. (2008) [2] also conducted an experimental study followed by a numerical simulation. In this work, a two-dimensional simplification of a three-dimensional setup is modeled in Ansys Fluent to study the steam condensation in the presence of non-condensable gases using geometry with the primary loop containing a square cross-section ($0.34 * 0.34$ m) and 2 m long test channel. The study concluded that the overall condensation rate is slightly underestimated compared to the experimental data. This underestimation was associated with the lower estimation of the local heat flux at the entrance of the steam-air mixture.

Kuhn (1995) [12] performed an experimental investigation of condensation in a vertical shell-in-tube test section, with almost the same geometrical dimension as Siddique, where he tested condensation of steam with and without non-condensable gases for a wide range of operational conditions. He concluded that condensation

in the presence of non-condensable gases has a dependency on the local liquid film Reynolds's number.

2.2 Numerical studies

Numerous numerical simulations on mass and heat transfer from partial condensation of pure or mixture (condensable or non-condensable) gases have been performed and reported, showing an acceptable agreement with its corresponding empirical formulation or experimental data. In most of these studies, annular and stratified flow pattern was assumed. Unfortunately, the simulation of full condensation, where other flow regimes like bubbly and slug flow may occur, has not been heavily investigated. Some articles related to condensation will be explained and discussed below.

N. Padoin and C. Soares [18] have carried out a theoretical investigation of condensation of saturated steam in a circular horizontal tube assuming a stratified flow regime. An acceptable correlation was obtained when comparing CFD results to the corresponding empirical formulation. Hyoungsoon Lee et. al. [15] investigated experimentally condensation in a vertical tube-in-shell heat exchanger using FR-72 as a working fluid along with a numerical simulation. A 2D axisymmetric computational domain of the 3D experimental model was used where a good agreement of heat transfer coefficient between CFD and experimental data was obtained.

Didi Zhang [24] has done experimental and numerical studies of R134a flow condensation in a pump-assisted separate heat pipe under the assumption of an annular flow regime. They performed the simulation adopting the Mixture- and Volume of Fluid (VoF) multiphase model and concluded that the VoF model is more suitable by providing a sharper interface.

In a study conducted by A. Badillo [23], a numerical simulation of condensation was performed using the VoF multiphase model on a 2D geometry with a structured mesh in Ansys Fluent. Three different models were employed and compared to represent the phase change associated with condensation: the *Lee* model, the *Heat flux balance equation* model, and the *Phase field* model. The research findings indicate that the Phase field model showed the highest reliability, as it displayed the least deviation between saturation temperature and interfacial temperature, followed by the Lee model.

More recently, P. Bhowmik [16] simulated partially steam condensation in STAR CCM+ software using a 3D geometry and validated the results from different runs against Kuhn experimental data. They reported/compared different quantities such as heat flux, centerline- and wall temperature. Good agreement can be seen for runs where a lower operational pressure (atmospheric) is used and disagreement when operational pressure is about 4-5 bar.

Chunxu Wu and Junming Li [17] conducted a simulation using Ansys/Fluent to model the full condensation of R32 in a 2D micro-channel. They employed the Volume of Fluid (VoF) method and the Lee condensation model in a transient mode. The primary goal of their research was to visualize a flow regime that closely matched the experimental results. Notably, in micro-channel condensation, the dominant force is surface tension, and the influence of gravity can be neglected in contrast to situations involving larger geometric scales.

Numerical studies of condensation can be summarized as follows;

- Ansys Fluent is widely being used
- Simulation of full condensation in a larger scale geometry where gravity is the predominant force has not been extensively investigated in commonly
- Combination of Volume of Fluid (VoF) method together with Lee model are commonly used for simulation of condensation
- Researchers have mainly focused on investigating the effect of non-condensable gases (air/helium) on HTC

3

Theory

This chapter provides a theoretical introduction to the heat transfer mechanism through condensation, including the relevant equations for film condensation. The governing equation solved in CFD single- and multiphase flow is introduced. This is followed by an overview of the commercial software utilized in the study.

3.1 Condensation

Condensation occurs when the temperature of a vapor is reduced below its saturation temperature. It is commonly achieved by making the vapor in direct contact with a cold surface. The latent heat of vaporization is released, and the condensate forms. Condensation can be divided into different modes such as *Film mode*, *Dropwise condensation on the surface* and *Direct condensation*. Here, a brief description of film condensation on a vertical surface will be given with relevant equations.

3.1.1 Film Condensation

Figure 3.1 shows schematically the process of film condensation on a vertical plate. The film thickness $\delta(y)$ (where y is the vertical downward coordinate) is given by:

$$\delta(y) = \left[\frac{4k_L(-\Delta T)\mu_L}{3\rho_L(\rho_L - \rho_V)g\mathcal{L}}\right]^{1/4} y^{1/4} \tag{3.1}$$

where k_l, μ_L and ρ_L represent the thermal conductivity, viscosity and density of the liquid. ρ_v is the density of the vapor and $\mathcal{L}$ is the characteristic length.

The local heat transfer coefficient reads:

$$\frac{\dot{q}(y)}{\Delta T} = \left[\frac{3\rho_L(\rho_L - \rho_V)g\mathcal{L}k_L^3}{4(-\Delta T)\mu_L}\right]^{1/4} y^{-1/4} \tag{3.2}$$

and the overall heat transfer coefficient for a plate of length ℓ can be calculated by:

$$\left(\frac{4}{3}\right)^{3/4}\left[\frac{\rho_L(\rho_L - \rho_V)g\mathcal{L}k_L^3}{(-\Delta T)\mu_L\ell}\right]^{1/4} \tag{3.3}$$

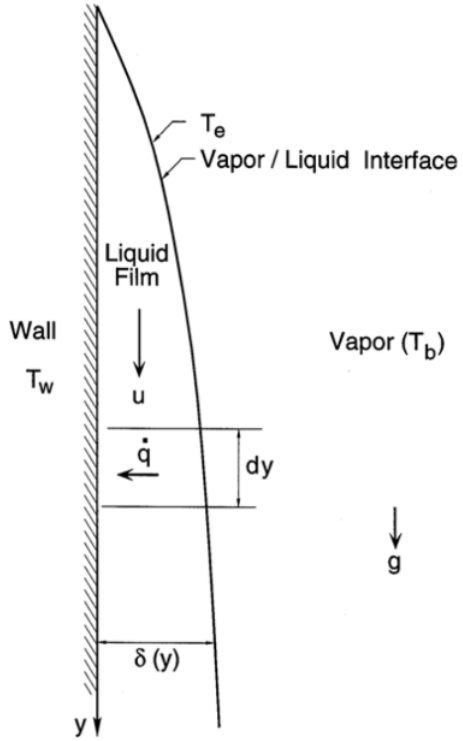

Figure 3.1: Sketch picture of film condensation (adopted from [8])

More details about assumptions that the equations are based upon and derivation of the equations can be found in literature [8].

3.2 CFD (Computational Fluid Dynamics)

Solving fluid dynamics problems numerically in a computer is called Computational Fluid Dynamics (CFD). It is a powerful tool in industrial application and academic research that has greatly been developed over several decades and is continuously made available to a broader user base every year.

3.2.1 Governing Equation

Fluid motion and heat transfer are governed by a set of equations for the conservation of mass, momentum, and energy called the Navier-Stokes equations. The density-normalized form of time-dependent three-dimensional fluid flow and heat transfer of an incompressible Newtonian fluid reads:

$$Continuity: \quad \frac{\partial \rho}{\partial t} + \frac{\partial \rho U_i}{\partial x_i} = 0 \tag{3.4}$$

$$Momentum: \quad \frac{\partial \rho U_i}{\partial t} + \frac{\partial \rho U_i U_j}{\partial x_j} = \rho g_i + F_i - \frac{\partial P}{\partial x_i} + \frac{\partial}{\partial x_j}\left(2\mu S_{ij}\right) \tag{3.5}$$

$$Energy: \quad \frac{\partial \rho E_0}{\partial t} + \frac{\partial \rho U_i E_0}{\partial x_i} = \rho U_i F_i - \frac{\partial q_i}{\partial x_i} + \frac{\partial}{\partial x_j}(U_i T_{ij}) \tag{3.6}$$

3.2.2 Mesh

When solving fluid dynamics problems numerically, the computational domain is divided into small control volumes. The governing differential equations are discretized and solved on each control volume in an iterative manner. Fluent Meshing provides different grid (element) types such as Polyhedral, Hexcore, Poly hexcore and Tetrahedral meshes. The polyhedral mesh has several advantages over Tetrahedral or hybrid meshes. The most important is through a lower overall cell count, with almost 3-5 times lower cell count for unstructured meshes compared to equivalent original tetrahedral mesh. Generally leading to faster solution convergence, and lower computational expense [7].

3.2.3 Reynold's Average Navier-Stokes (RANS)

The time-averaged Navier-Stokes equations are based on the assumption that all variables can be separated into a mean and fluctuation component, $\bar{\Phi}_i$ and $\Phi_i^{'}$ (see Eq. 3.7). This is commonly called Reynold's decomposition.

$$u_i = \bar{u_i} + u_i^{'} \tag{3.7}$$

Inserting the decomposition into the steady-state NS equations, the continuity equations 3.8 and momentum equations 3.9 yields:

$$\frac{\partial v_i}{\partial x_i} = 0 \tag{3.8}$$

$$\rho \frac{\partial \bar{v_i} \bar{v_j}}{\partial x_j} = -\frac{\partial \bar{p}}{\partial x_i} + \rho \frac{\partial}{\partial x_j}\left(\mu \frac{\partial \bar{v_i}}{\partial x_j} - \rho \overline{v_i' v_j'}\right) \tag{3.9}$$

The last term in Eq. 3.9, $\overline{v_i' v_j'}$, is called Reynolds stress tensor. This term arises as a consequence of the time-averaging of NS, and it needs to be modeled to close the system of equations.

There are many models available in Fluent to close the system of equations. The most frequently used are $k-\epsilon$ (suitable for the inner boundary layer) and $k-\omega$ (good in the outer region of the boundary layer and outside of it). The standard version of SST $k-\omega$ is a combination of $k-\epsilon$ and $k-\omega$ turbulence models that have been modified for a wider class of flows [9]. Didi Zhang [24] employed both the $k-\epsilon$ and SST $k-\omega$ turbulence models when modeling condensation. By comparing the results with experimental data, they found out that the SST $k-\omega$ model gave a better correlation. Therefore, the SST $k-\omega$ turbulence model is adopted in this study.

3.2.4 Near wall treatment

The boundary layer near the wall in a turbulent flow can be divided into three different regions, see Figure 3.2, where the dimensionless wall distance, y^+, is used to define the range in which different regions are characterized. The viscous region, $0 < y^+ < 5$ (dominate by viscous diffusion), logarithmic region, $y^+ > 30$ (dominate by turbulent diffusion), and buffer region $5 < y^+ < 30$ (acts as a transition region between these two regions where the viscous diffusion of streamwise momentum is gradually replaced by turbulent diffusion) [9].

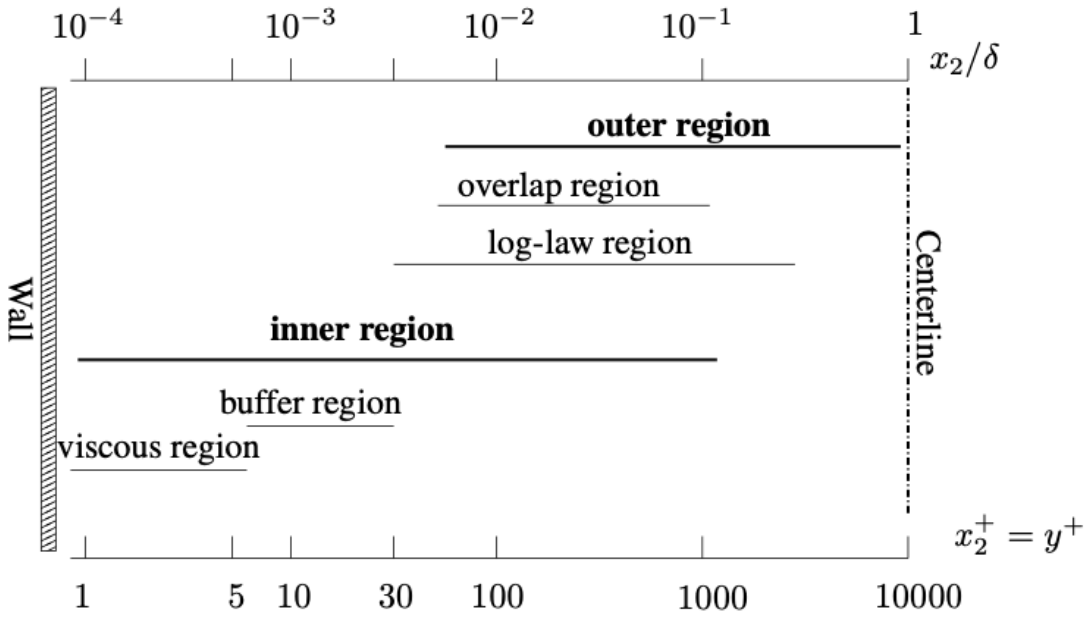

Figure 3.2: The wall region (adopted from [10])

There are two options for treating the near-wall regions. *Wall function*, where a coarse mesh near the wall is used assuming that the logarithmic law is applied, and *Low Reynolds number model* where a fine mesh near the walls is used, and the turbulence model is modified to account for the viscous effect respectively.

However, when the flow near walls dominates the physics, using the wall function when predicting heat transfer is usually not recommended. This is because the heat transfer to the fluid is dictated by grid resolutions close to the wall. When choosing to use *Low Reynolds number model*, a sufficiently large amount of grid element must be inserted near any solid boundary so the boundary layer can be adequately resolved. Therefore, a $y^+ < 5$ (ideally ≈ 1) is appreciated [9].

3.3 Multiphase Flow Modelling

Multiphase flow modeling is characterized by a simultaneous flow of any liquid, gas, and solid combination in the region of interest. When solving multiphase flow

problems numerically in a CFD solver, a number of selections need to be done that closely mirror the physical characteristics of the flow. To this end, factors such as flow regime and type of phase coupling between dispersed and carrier phases need to be described in detail. This section will present the fundamental aspect of the multiphase flow.

In Ansys Fluent [5], two different formulations of the Navier-Stokes equations are available (i.e., Eulerian and Lagrangian formulations). In the Eulerian formulation, a fixed spatial grid is used to analyze fluid flow, and data is collected at specific points in space over time, while in the Lagrangian formulation, an individual fluid particle or particle of interest is tracked as it moves through space and time.

When it comes to the simulation of condensation, the interface between liquid and vapor becomes diffuse, meaning there is no clear, well-defined boundary. In this scenario, both the liquid and vapor phases can be mathematically treated as interpenetrating continua. In such cases, the Eulerian approach is a convenient option, which many researchers have employed in this content.

3.3.1 Fluid Flow Regime

Condensation is a complicated physical phenomenon that is characterized as a two-phase flow. In addition to viscous, inertia, and pressure forces that are predominant in single-phase flow, two-phase flow is affected by other forces such as interfacial surface tension, lift, drag, virtual mass, etc., as well as the exchange of mass and momentum, further increasing the complexity of the process. A general definition of two-phase flow, typically liquid-gas through a system like a pipe or a channel simultaneously, is given by [8], which includes;

- *bubbly flow*: in which the gas is present within the liquid in the form of innumerable bubbles of small size
- *slug flow*: where individual gas bubbles merge to form a large gas mass or slug that is often cylindrical in shape
- *stratified flow*: where the gas and liquid regions are separated, with the gas that is lighter flowing on top of the heavier liquid
- *annular flow*: where one fluid (typically the liquid) occupies the space adjacent to the tube wall and surrounds the other fluid (gas) that flows in the center of the tube

Depending on the operational conditions and the properties of the working fluids, one or some of those mentioned above and shown in figure 3.3 flow regime may occur.

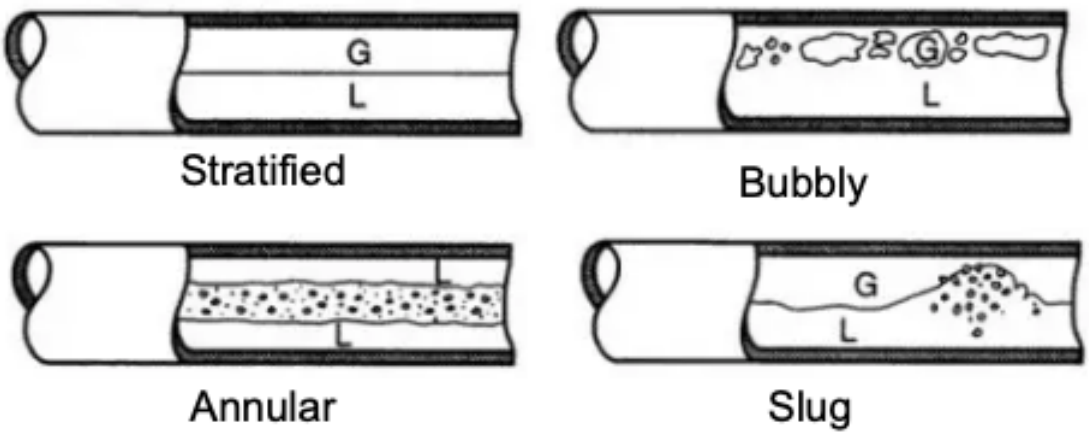

Figure 3.3: Sketches of flow regimes, (Adopted from [8])

3.3.2 Phase Coupling

The interaction between phases can be categorized as (1) one-way coupling: the dispersed phase does not affect the continuous phase, there is no communication between the dispersed phase, and the governing equations are solved for the continuous phase, and the dispersed phase is tracked afterward. (2) Two-way coupling: The dispersed phase affects the continuous phase through momentum transfer and volume fraction. (3) Four-way coupling: The continuous phase is affected by the dispersed phase and communication between the dispersed phase.

3.3.3 Stokes Number

The Stokes number is a dimensionless number used to estimate the ratio of a dispersed-phase timescale to a continuous-phase timescale. The turbulent Stokes number is defined as [3]:

$$St_T = \frac{\tau_d}{\tau_T} \tag{3.10}$$

where τ_d is the timescale of the dispersed phase and τ_T is the relevant timescale of turbulence, which can be written as:

$$\tau_d = \frac{\rho_d D^2}{18\mu_f} \tag{3.11}$$

$$\tau_T = \frac{k}{\epsilon} \tag{3.12}$$

For the flow in which St_T tends to zero ($St_T \to 0$), it indicates that the particles follow the flow completely, and when ($St_T \to \infty$), the behavior of the particles is not correlated with the flow characteristics as seen in Figure 3.4.

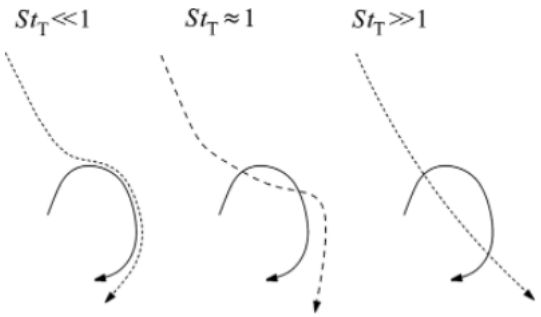

Figure 3.4: Effects of a turbulent eddy (solid line) on particle trajectory (dashed line) for different Stokes-number limits, (adopted from [4])

3.3.4 Eulerian Formulation

In the Eulerian type of formulation, several mathematical approaches (i.e., Eulerian-VoF- and Mixture multiphase model) can be selected depending on flow physics, level of accuracy, and computational cost. Below is a brief description of the advantages and disadvantages of the Mixture- and VoF methods employed in this study, including the relevant governing equation.

3.3.5 Mixture Multiphase Model

The Mixture Multiphase, MM, model is a simplified version of the full Eulerian Multiphase, EM, model by solving the continuity, momentum, and energy equations for the whole mixture, and the volume fraction equation is solved for the secondary phase. It can be used to model multiphase flow where different phase moves at different velocities and for homogeneous multiphase flow where the slip (relative) velocity between phases is zero. However, the assumption of a local equilibrium over a short spatial length scale should be fulfilled.

The MM model is a good substitution for the full Eulerian model when there is a wide distribution of the particulate phase. The MM model solves fewer variables than the full Eulerian model. Hence, it is less accurate but simpler to converge and more stable. Therefore, starting with and eventually using it as an initial condition for the full Eulerian model can be a good option. The governing equation solved in this model reads [6]: The continuity equation for mixture:

$$\frac{\partial}{\partial t}\left(\rho_m\right) + \nabla \cdot \left(\rho_m \overrightarrow{v_m}\right) = 0 \tag{3.13}$$

where $\overrightarrow{v_m}$ and ρ_m are mass-averaged velocity and mixture density, respectively.

The momentum equation for the mixture is obtained by summing the individual momentum equation for all phases:

$$\frac{\partial}{\partial t}\left(\rho_m \overrightarrow{v_m}\right) + \nabla \cdot \left(\rho_m \overrightarrow{v_m} \overrightarrow{v_m}\right) = -\nabla p + \nabla \cdot \left[\mu_m \left(\nabla \overrightarrow{v_m} + \overrightarrow{v_m}^T\right)\right] + \rho_m \overrightarrow{g} + \overrightarrow{F} - \nabla \cdot \left(\sum_{k=1}^{n} \alpha_k \rho_k \overrightarrow{v}_{dr,k} \overrightarrow{v}_{dr,k}\right) \tag{3.14}$$

where n is the number of phases, $\overrightarrow{F}$ is the body force, μ_m is the viscosity of the mixture, ∇p is the pressure gradient, g is the gravitational force, α_k is volume fraction and $\overrightarrow{v}_{dr,k}$ is the drift velocity.

3.3.6 Volume of Fluid (VoF) Multiphase Model

The VoF model is a surface-tacking technique applied to fixed grids. In this model, a single set of momentum equations is solved for all phases, and the volume fraction of each phase in each computational cell is tracked throughout the domain. The method is based on the fact that two or more fluids are not interpenetrating, and a new variable will be introduced for each additional phase in the model. In each cell, the sum of the volume fraction of all phases equals unity, and the volume fraction in any given cell takes a value from 0 to 1. The continuity equation of the volume

fraction for phase q has the following form:

$$\frac{1}{\rho_q}\left[\frac{\partial}{\partial t}\left(\alpha_q \rho_q\right) + \nabla \cdot \left(\alpha_q \rho_q \overrightarrow{V_q}\right) = S_{\alpha_q} + \sum_{p=1}^{n}\left(\dot{m}_{pq} - \dot{m}_{qp}\right)\right] \tag{3.15}$$

where $\dot{m}_{qp}$ and $\dot{m}_{pq}$ is the mass transfer from phase q to phase p and phase p to phase q, respectively. ρ_q, $\overrightarrow{V_q}$, and S_{α_q} are the density, velocity, and source term of the phase q, respectively.

The volume fraction equation will not be solved for primary-phase, but it is computed based on the following constraint:

$$\sum_{q=1}^{n} \alpha_q = 1 \tag{3.16}$$

There are two different formulations for the volume fraction equation, Implicit and Explicit, and the implicit one has the following form:

$$\frac{\alpha_q^{n+1}\rho_q^{n+1} - \alpha_q^n \rho_q^n}{\Delta t} V + \sum_f \left(\rho_q^{n+1} U_f^{n+1} \alpha_{q,f}^{n+1}\right) = \left[S_{\alpha_q} + \sum_{p=1}^{n}(\dot{m}_{pq} - \dot{m}_{qp})\right] V \tag{3.17}$$

where $n+1$ and n are the current and previous time steps, respectively, U_f^{n+1} is the volume flux through the face at time step $n+1$, and V is cell volume. Since the volume fraction at the current time step is a function of other quantities at the current time step, a scalar transport equation is solved iteratively for each of the secondary-phase volume fractions at each time step[6].

3.3.7 Lee Condensation Model

Mass transfer during the condensation process can be handled in one of two ways in Fluent (i.e., using *Lee-* or *Thermal Phase Change* model). However, the Lee model is the only one compatible with the Mixture- or VoF method, which is used in this work. The vapor-transport equation governs the liquid-vapor mass transfer [6].

$$\frac{\partial}{\partial t}(\alpha_v \rho_q) + \nabla \cdot (\alpha_v \rho_v \overrightarrow{V_v}) = \dot{m}_{lv} - \dot{m}_{vl} \tag{3.18}$$

where the source terms in equation 3.18 are defined as:

For evaporation ($T_l > T_{sat}$)

$$\dot{m}_{lv} = coeff * \alpha_l \rho_l \frac{T_l - T_{sat}}{T_{sat}} \tag{3.19}$$

For condensation ($T_v < T_{sat}$)

$$\dot{m}_{vl} = coeff * \alpha_l \rho_l \frac{T_{sat} - T_v}{T_{sat}} \tag{3.20}$$

and T_{sat} is the saturation temperature for the fluid. The mass transfer intensity, (*coeff*) in Eq. 3.19 and 3.20 with the unit $[1/s^1]$, is a time relaxation factor that defines the rate at which the mass is transferred from one phase to the other during phase change. This empirical coefficient can take values as low as 0.001 up to 10^7. In the literature, a wide range of values has been reported, and it is dependent on many factors, e.g., operational condition, mesh size, and time step. A common observation in all the studies in this field is that a low value of *coeff* leads to a deviation between the saturation- (T_{sat}) and interfacial (T_i) temperature, whereas a high value causes convergence problems.

In this study, the usage strategy for utilizing the mass transfer intensity (*coeff*) has been as follows: Initiate the simulation with the default value (i.e., 0.1), and thereafter, it is systematically updated and increased alongside the increase of condensate water on the inner surface of the tube.

3.4 Commercial Software

In this section, the software used in this thesis work is described. Ansys Discovery Modeling is used for creating geometries, Ansys Fluent Meshing is used for mesh generation and the CFD commercial software Ansys Fluent is used for the simulations.

3.4.1 ANSYS Fluent Mesh

Ansys Fluent Mesh is a robust, modern, unstructured mesh generation program that can handle unlimited size and complexity meshes. Meshes may include tetrahedral,

hexahedral, polyhedral, prismatic, or pyramidal cells. Unstructured mesh generation techniques pair basic geometric building blocks with extensive geometric data to automate the mesh generation process.

There are two principal approaches to creating meshes in Ansys Fluent Meshing; (1) Generate a tetrahedral, hexcore, or hybrid volume mesh from an existing boundary mesh, or (2) Generate a tetrahedral, hexcore, or hybrid volume mesh based on meshing objects from a faceted geometry (from CAD or the *.tgf* format from Ansys Meshing).

3.4.2 Ansys Fluent

Ansys Fluent is a state-of-the-art computer program to model fluid flow, heat transfer, and chemical reactions in complex geometries. It provides comprehensive modeling capabilities for incompressible and compressible, laminar, and turbulent fluid flow problems. Steady-state or transient analysis can be performed. In Ansys Fluent, a broad range of mathematical models for transport phenomena (like heat transfer and chemical reactions) is combined with the ability to model complex geometries. Examples of Ansys Fluent applications include laminar non-Newtonian flows in process equipment, conjugate heat transfer in turbomachinery, and automotive engine components [6].

4
Methodology

This chapter outlines geometries, methodology, and boundary conditions for different cases. This chapter also describes the mesh convergence study on the first test case (i.e., Pipe flow) and convergence criteria used to achieve a converged solution, followed by a description of different attempts for the second test case (i.e., the Kuhn test case).

4.1 Pipe Flow

4.1.1 Geometry and Simulation Conditions

The geometry of the *Pipe flow* is shown in Figure 4.1 and is selected to be as close as possible to the *Kuhn test case*. The length and diameter are equal to 100 and 49 mm, respectively. Aluminum with a smooth surface is used as wall material, and air as working fluid where $Re = 24.5 * 10^3$, with physical properties summarized in Table 4.1. The simulation is carried out with the simulation settings and boundary conditions according to Table 4.2.

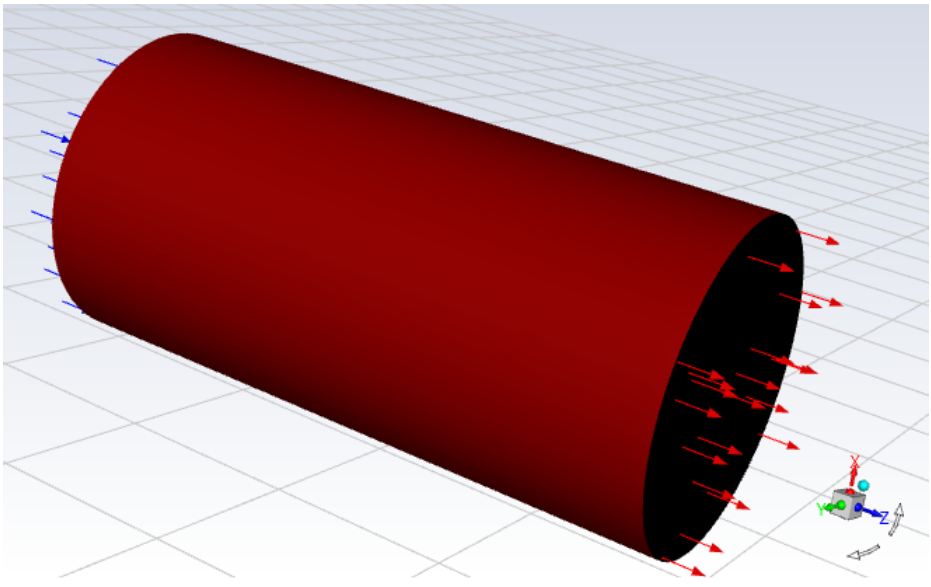

Figure 4.1: Geometry used for test case 1, inlet velocity marked as blue arrows and pressure outlet marked red arrows

	Air	Aluminium
$\rho \quad kg/m^3$	1.225	2719
$C_p \quad J/(kg.K)$	1006.43	871
$k \quad W/(m.K)$	0.0242	202.4
$\mu \quad kg/(m.s)$	$1.79.10^{-5}$	#

Table 4.1: Materials properties used in test case 1

Simulation Settings	**Boundary Condition**
Pressure-based solver	Inlet-outlet periodic boundary
Pseudo transient time step	Upstream bulk temperature = 300K
Coupled as pressure-velocity scheme	Wall temperature = 290K
SST k-ω as turbulence model	Inlet velocity = 7.3 m/s
2nd order upwind as discretization scheme	No slip at the wall
Hybrid initialization	Outlet pressure set to 0 gauge

Table 4.2: Simulation settings and boundary condition used for test case 1

4.1.2 Mesh Study

A mesh convergence study is performed on the first test case by considering various quantities, such as pressure drop and wall shear stress, as a function of the total number of cells and boundary layer resolutions. In order to achieve a mesh-independent result, four different meshes are constructed with a cell count between 12.7 to 281 thousand with the same convergence criteria. These are referred to as *Mesh 1* to *Mesh 4* in Table 4.3. A Polyhedral mesh is used for the spatial discretization of the domain, and the near-wall regions were refined, adopting prism layers with a growth rate of 1.2.

As it is shown in Table 4.3, the quality of the mesh is verified by looking into minimum orthogonality and maximum cell skewness. Generally, the orthogonality and skewness should be higher and less than 0.1 and 0.85 respectively which is the case here. Starting from *mesh 1*, as a baseline, the mesh is refined by reducing the height of the first cell while the number of boundary layers and the total number of cells are increased leading to an overall lower value of y^+.

	Mesh 1	Mesh 2	Mesh 3	Mesh 4
Total number of cells	12.7k	52.7k	187k	281k
Min orthogonality	0.2	0.35	0.18	0.15
Max skewness	0.22	0.20	0.21	0.22
First cell height [mm]	0.25	0.15	0.1	0.05
y^+	3.7	2.1	1.38	0.7
Number of prism layers	10	15	20	23

Table 4.3: Numerical parameters of grid convergence study for the first test case (Pipe flow)

Equations 4.1 (pressure drop) and 4.2 (wall shear stress) have been used to validate the results obtained from the simulation. The friction factor, f_D, is obtained from the Moody Chart diagram assuming smooth pipe. L and D are the length and diameter of the pipe respectively. ρ and V are the density and velocity of the air, respectively.

$$\Delta P = f_D \frac{L}{D} \frac{\rho V^2}{2} \tag{4.1}$$

$$\tau_w = \frac{f_D \rho V^2}{8} \tag{4.2}$$

4.2 Kuhn Test Case

The second test case is adopted from *Kuhn's Experimentally Investigation of Heat Transfer from Condensing Steam Gas Mixture and Turbulent Film Flowing Downward Inside a Vertical Tube (1995)* [12]. Kuhn conducted 137 runs, using various operational conditions for each run. During "RUN 1.1-5R1," full condensation of pure water vapor occurred. Kuhn has reported quantities such as static temperature at the centerline and inner wall of the condenser tube, as well as the rate of condensate water at different axial locations along the tube.

4.2.1 Computational Domain

An overview of the experimental test section used by Kuhn is shown in Figure 4.2. It consists of a double tube annulus fitted with thermocouples mounted on inner and outer walls to measure local temperatures. The steam flows in the downward direction in the inner tube. Cooling water is injected through four inlets and flowing upwards. Between the annulus and outer flow, a steel pipe separates the flow. The geometry has been divided and simplified into three different sub-geometries (configurations), which will be described in the next section.

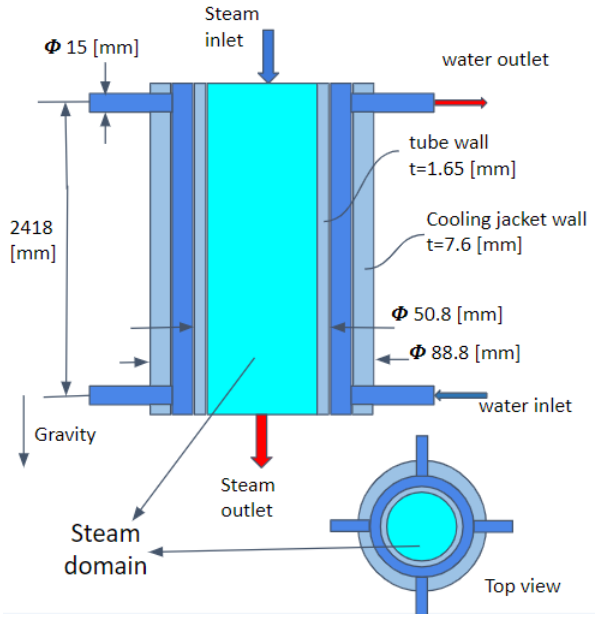

Figure 4.2: Sketch of test section dimension and components used in Kuhn test section. The image is not according to the schedule

4.2.2 Geometry Configuration

This study has used three different geometry configurations to investigate the numerical challenges when modeling full condensation. Due to difficulties in getting full condensation, it has been simplified by considering only the steam domain (i.e., excluding the water domain, cooling jacket, and tube wall), shown in Figure 4.4, and using heat flux at tube-wall as a boundary condition. However, using heat flux as a tube-wall boundary condition gives rise to other issues, which made us include all parts with some modifications, shown in Figure 4.5; thus, using a half-section circumferentially symmetric of the whole geometry to save some computational time. The steam domain has been extended at the inlet to let the flow develop before the condensing section, and adopting more cells across the tube wall as it is considered the most critical region in the entire geometry. The reason behind these configurations will be explained in the results section.

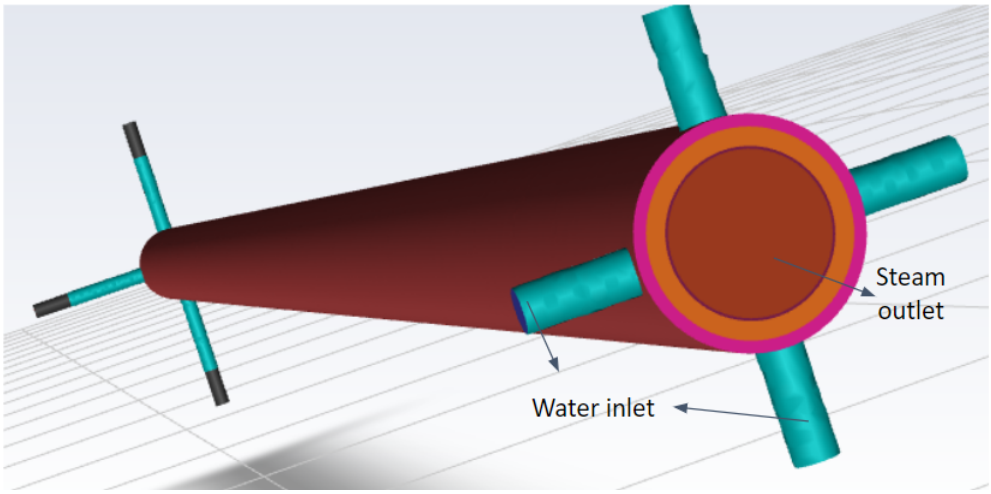

Figure 4.3: Configuration 1: Full geometry

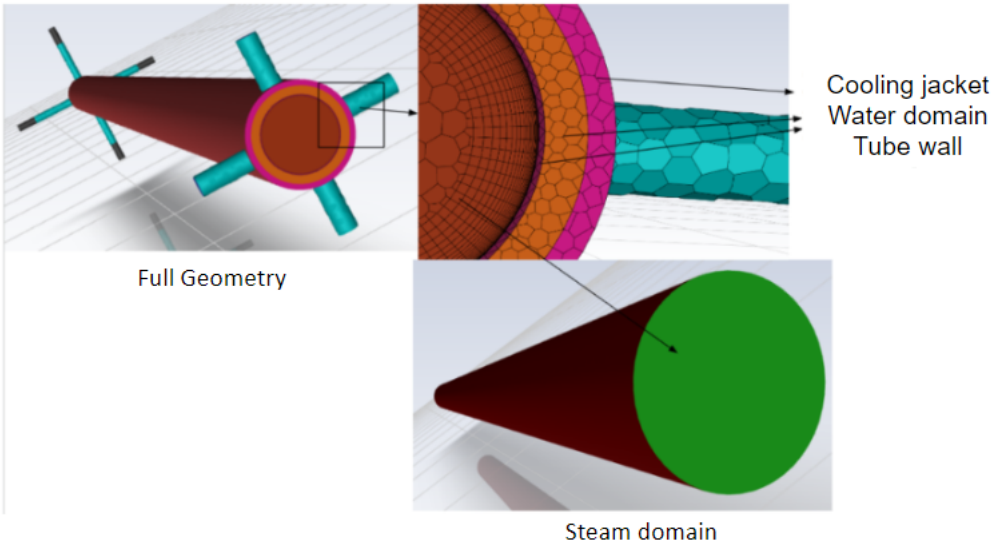

Figure 4.4: Configuration 2: Only steam domain, i.e. excluded the cooling jacket, water domain, and tube-wall

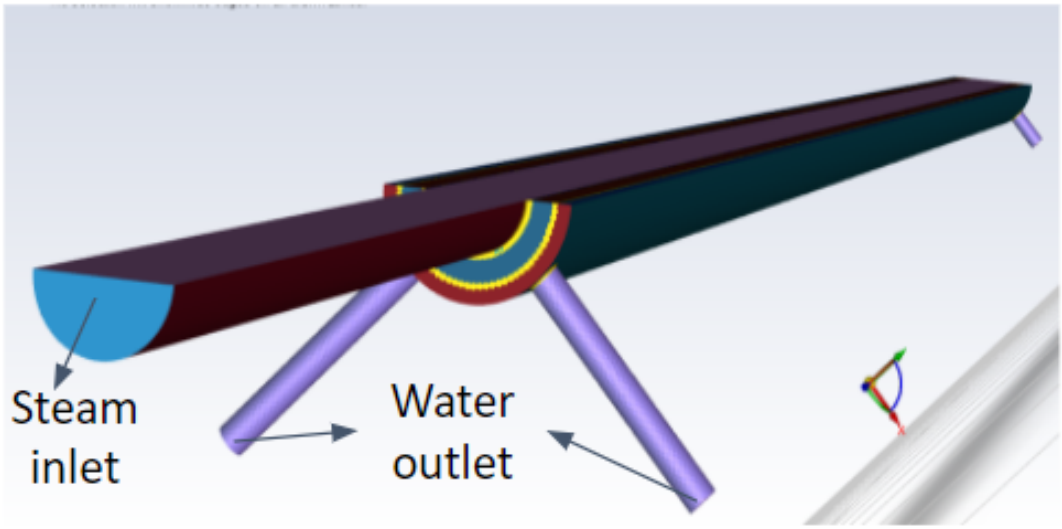

Figure 4.5: Configuration 3: Half-section of full geometry, the steam domain is extended at inlet

4.2.3 Mesh

Polyhedral mesh is used for all configurations in the Kuhn test case, as it performed well in the pipe flow case. Figure 4.6 shows the mesh used in configuration 3 with the properties summarized in Table 4.6. The mesh properties for two other configurations are summarized in Table 4.4 and 4.5, respectively. All meshes have been created using *watertight workflow* in Fluent Mesh. The surface mesh is created using *Curvature & Proximity* Size Function, and prism layers are generated using *uniform* as Offset Method Type.

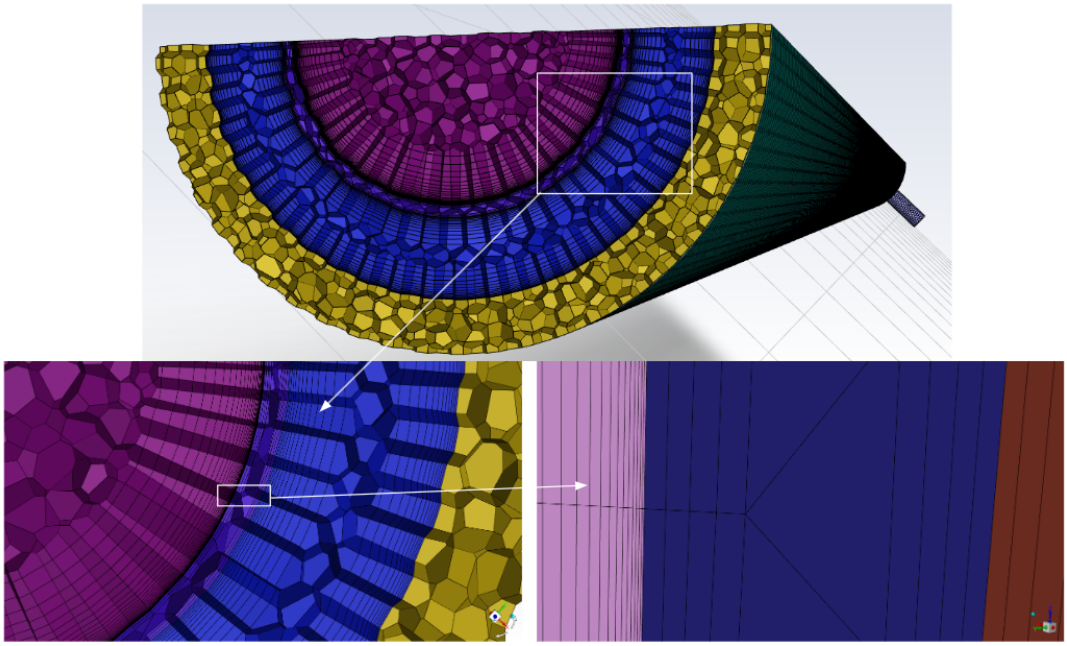

Figure 4.6: Mesh used for configuration 3

Quantities	Value	Quantities	Value
Total N.o cells	4,167,104	N.o prism layers (water domain)	5
Min orthogonality	0.2	N.o prism layers (steam domain)	20
Max skewness	0.2	y^+ (steam side)	1.5
Growth rate	1.2	y^+ (water side)	3.2

Table 4.4: Mesh properties in configuration 1

Quantities	Value	Quantities	Value
Total N.o cells	1,033,910	N.o prism layers	20
Min orthogonality	0.2	Growth rate	1.19
Max skewness	0.11	y^+	1.5

Table 4.5: Mesh properties in configuration 2 (only steam domain)

Quantities	Value	Quantities	Value
Total N.o cells	2,462,742	N.o prism layers (water domain)	12
Min orthogonality	0.15	N.o prism layers (steam domain)	27
Max skewness	0.12	y^+ (steam side)	1
Growth rate	1.2	y^+ (water side)	2.4

Table 4.6: Mesh properties in configuration 3

4.2.4 Boundary Conditions and Fluid Properties

The boundary conditions used in the Kuhn test case are shown in Table 4.8. P_{inlet} and T_{inlet} are inlet pressure and temperature respectively. Ws is the vapor mass flow rate, and Wc is the water mass flow rate. In order to avoid the inlet effects and to obtain a fully turbulent flow, the velocity profile is specified through a power law for the steam flow according to Eq. 4.3

$$\frac{u}{U_{max}} = \left(1 - \frac{r}{R}\right)^{1/n} \tag{4.3}$$

where n is equal to 7, u is inlet mean velocity, U_{max} is inlet max velocity, r and R are local radius and pipe radius respectively. For configuration 2, a constant heat flux of 11798 W/m^2. The heat flux is calculated using water temperature difference at inlet-outlet from experimental data, and it is specified at tube-wall-condition where the effect of wall conduction has been neglected.

Water-liquid is selected as the primary (continuous), water-vapor as the secondary (dispersed) phase, and steel as the wall material. The physical properties are summarized in Table 4.7 and are taken from the NIST website [22].

Quantities	Water-vapor	Water-liquid	Steel
$\rho \quad kg/m^3$	2.55	998.2	8030
$C_p \quad J/(kg.K)$	Piece-wise linear	4182	502.48
$k \quad W/(m.K)$	0.0261	0.6	16.27
$\mu \quad kg/(m.s)$	$1.34 * 10^{-5}$	$1.003 * 10^{-3}$	#
Standard State Enthalpy $J/kgmol$	$3.86.10^7$	0	#

Table 4.7: Materials properties used in Kuhn test case

#	P_{inlet} $[kPa]$	T_{inlet} $[K]$	Ws $[kg/hr]$	Wc $[kg/hr]$
Run 1.1-5R1	501.3	424.45	61.3	1074

Table 4.8: Boundary condition used in Kuhn test case

4.2.5 Mathematical Approach

For the Kuhn test case, the Mixture- and VoF (Volume of Fluid) multiphase models are used to solve the hydrodynamics of the two-phase flow, i.e., mass, momentum, and heat transfer along with the Lee model to handle the phase change (condensation) phenomena. The governing equations are presented in the theory section, where an implicit formulation for the volume fraction is used, and the phase interface is treated as dispersed. The effect of surface tension is neglected as it does not play a significant role when the effect of gravity is taken into account.

Initially, the Mixture multiphase model, due to its simplicity, is used in configurations 1 and 2 under steady-state assumption. An additional transient scheme is used for configuration 2 to account for time-dependent behavior. The Volume of Fluid (VoF) method is employed in the final configuration, still assuming a steady state. The VoF method is likely chosen for its ability to capture fluid interfaces accurately. These cases are referred to as configurations 1, 2, and 3 and are summarized in Table 4.9.

#	Multiphase model	Mode
Configuration 1	Mixture	Steady-state
Configuration 2	Mixture	Steady-state & Transient
Configuration 3	VoF	Steady-state

Table 4.9: The solver configuration that is applied in this study

4.2.6 Solver Settings

The numerical solver setting that is used in all simulations follows as a Pressure-Based solver. The turbulence fluctuation is modeled using the SST $k-\omega$ turbulence model. The coupled scheme is used for Pressure-Velocity coupling with a

Global Time Step. The second-order upwind scheme is used to describe the momentum, volume fraction, turbulent kinetic energy, specific dissipation rate, and energy. PRESTO! scheme is used for the pressure and a Least Squares Cell-based scheme for the gradients.

These settings are in general and have been changed during simulation to achieve convergence with solution stability. Many factors directly/indirectly affect the convergence of the solution, such as the under-relaxation factor or time-step (when running in fully transient mode), which has been modified case dependently, and therefore, no specific value can be given.

5

Results and Discussion

The results obtained from **Pipe Flow Case** and **Kuhn Test Case** are generally presented in terms of velocity- temperature- and water volume fraction fields and profile in the condensing section.

5.1 Pipe Flow Case

The residual convergence of the case is shown in Figure 5.1 along with the wall shear stress variation as a function of iterations. The residuals, with a cut-off at 10^{-6}, and the rate of change in the wall shear stress are used as convergence criteria to judge the convergence.

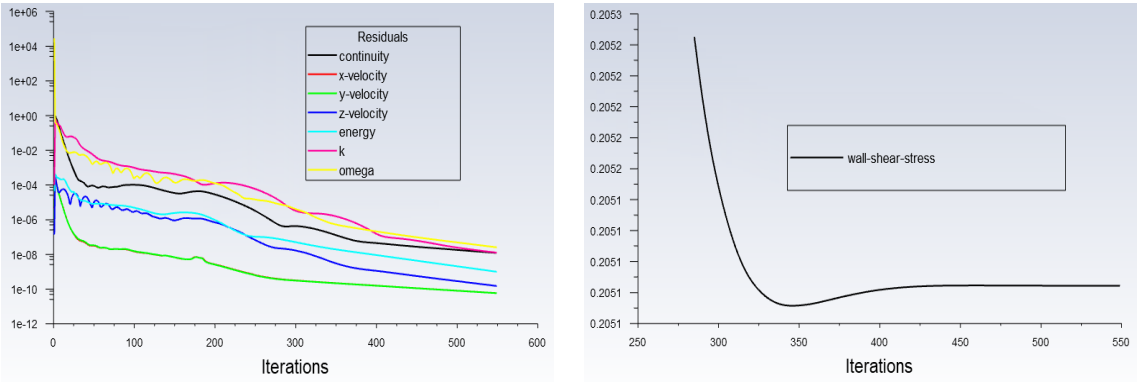

Figure 5.1: Convergence criteria: residuals cutoff sett to 10^{-6} (left) and variation wall shear stress as a function of iterations (right)

Figure 5.2 shows the fluctuation of the wall shear stress for the selected meshes. Relative convergence of the results is obtained as the total number of cells passes 187 thousand. Hence, using *Mesh 3* (see Table 4.3) is judged to give mesh independent results.

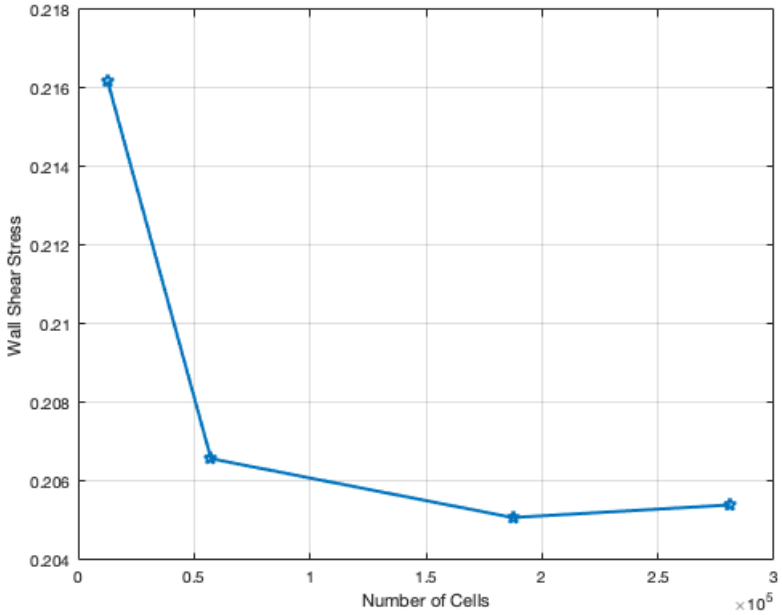

Figure 5.2: Mesh independence test

The CFD results using mesh 3 (see Table 4.3) are compared to the corresponding analytical solution to assess the reliability of the simulation results. As seen in Table 5.1, a good correlation is obtained for the pressure drop and wall shear stress with a deviation of less than 1.5 %. Figure 5.3 shows the static temperature and velocity profiles at three locations along the pipe. A slight temperature drop is observed due to heat removal at the wall, while a constant velocity profile is seen because of the inlet-outlet periodic boundary.

Variables	CFD	Analytical
Pressure drop [Pa]	1.67	1.64
Wall shear stress [Pa]	0.2050	0.2020

Table 5.1: Comparison between CFD vs analytical results of pressure drop and wall shear stress

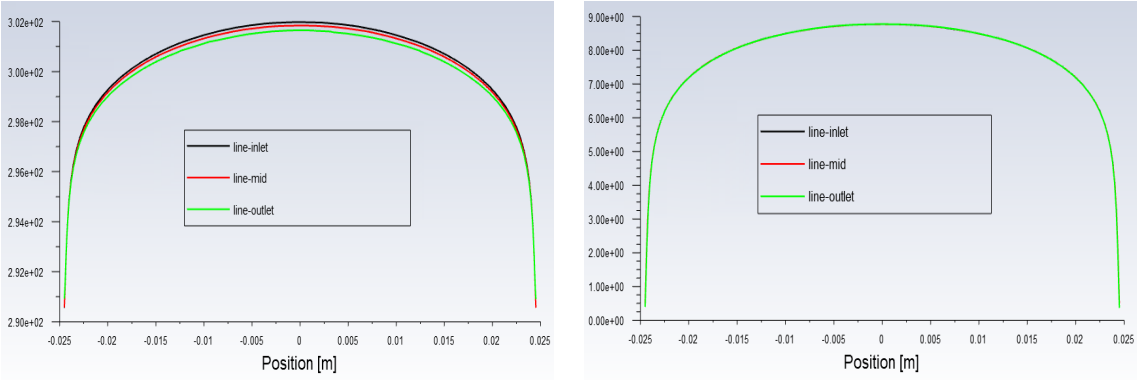

Figure 5.3: Static temperature- (left) and velocity (right) profile at the inlet (black), middle (red), and outlet (green) line in the pipe

5.2 Kuhn Test Case

The Kuhn experimental data is utilized as a reference for the simulation of full condensation. Three different modeling configurations, see Table 4.9, are evaluated and will be presented below. Although the simulation of full condensation has not been reached through this study, it is promising that the CFD simulation captured a thin water film along the entire inner surface of the condensing region that grows downstream.

5.2.1 Configuration 1

Figure 5.4 shows the water volume fraction at the outlet of the steam domain when the Lee coefficient (*coeff*) is gradually increased to a value of 70. At this point, the thickness of the water film, shown in Figure 5.4 (c), is approximately 0.2 mm, and a further increase in the value of *coeff* will trigger an imbalance in mass and energy conservation.

In order to increase the stability of the simulation, a transient simulation is also conducted. Since transient simulation requires a significantly higher computational effort, the geometry is simplified by considering only the condensing domain, where constant heat flux is used at the tube wall.

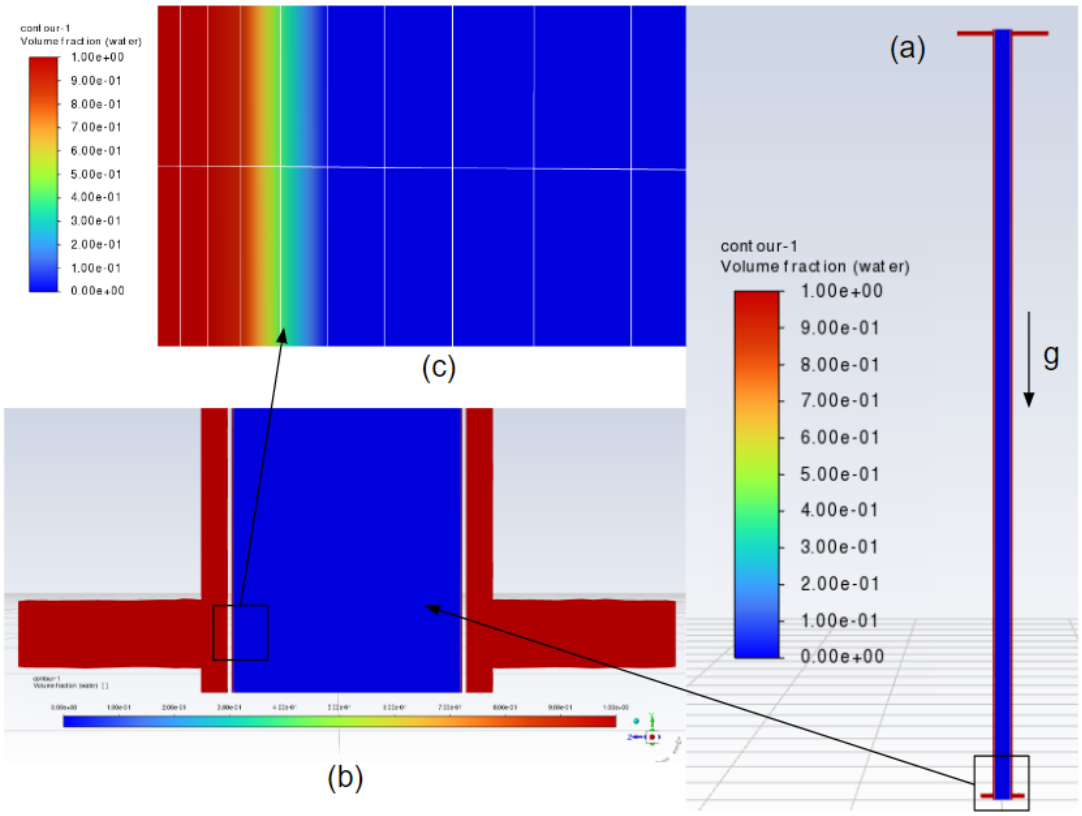

Figure 5.4: Contour plot of water volume fraction, red and blue color represents water and steam respectively

5.2.2 Configuration 2

When applying a constant heat flux to the wall, Figure 5.5 (a) illustrates that the temperature distribution along the entire tube wall shows non-uniform behavior. A non-physical low temperature is observed at the wall downstream of the inlet (see Figure 5.5 (b)). This causes the mass transfer rate, Figure 5.5 (d), to become very high, which indicates an intense condensation in this region while the water volume fraction, see Figure 5.5 (c), is almost zero. Increasing the value of *coeff* can mitigate it (i.e., the lowest temperature value increases), but it still does not solve the problem entirely. Furthermore, the condensate water film within the domain does not exceed a thickness of 0.2 mm at any location.

In addition to the problem mentioned above, there are other issues concerning the velocity field. Figure 5.6 (b) shows the mixture velocity magnitude in the 0-1 m/s range at the outlet cross-section where a high-velocity magnitude is visible at the water and steam interface. A possible reason for the non-physically high velocity can be the flow Stokes number assumption that the Mixture model relies on (i.e., $St \ll 1$). As an investigation, the bubble diameter initially used 0.1 mm for the dispersed phase also decreased to 10^{-3} mm. However, no significant improvement in the results is observed in the gas-liquid interface.

The results based on the configuration 2 setup are all from a steady-state simulation. One transient simulation of the already-mentioned problems is also conducted. However, it only shows a delayed effect.

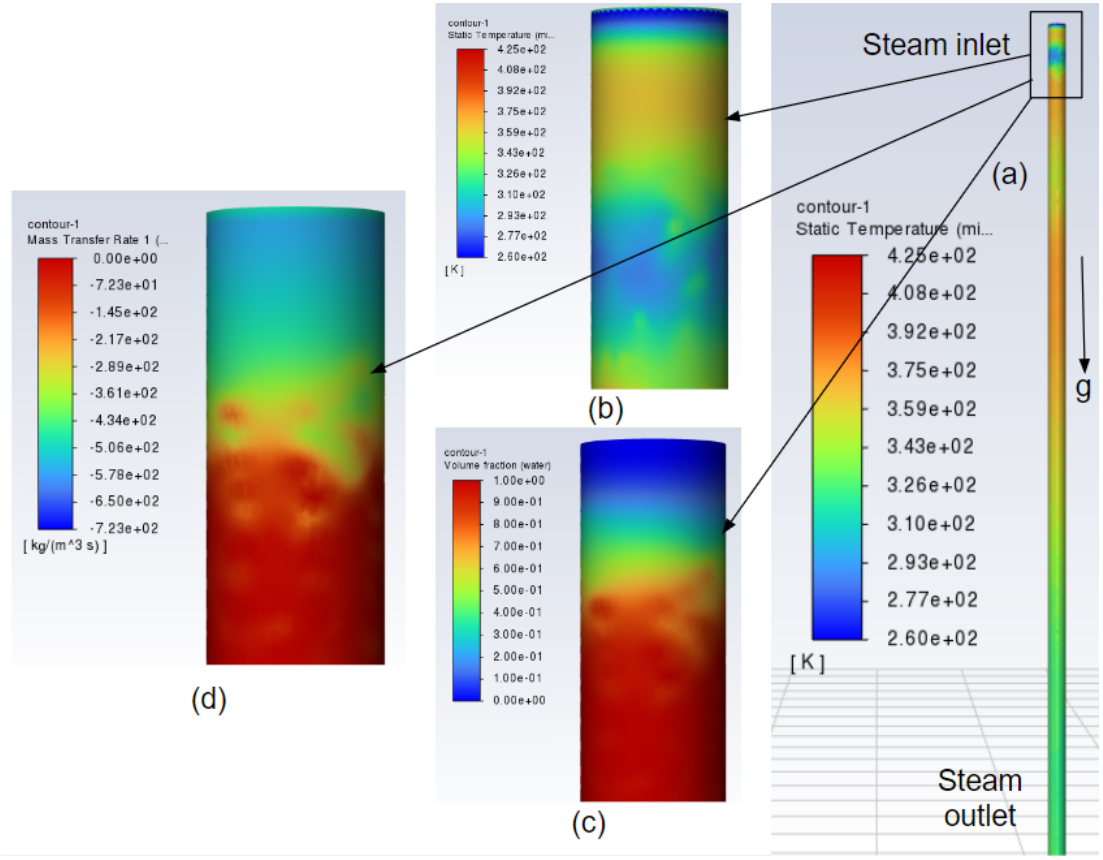

Figure 5.5: (a) and (b); contour plot static temperature, (c); water volume fraction, (d); mass transfer rate

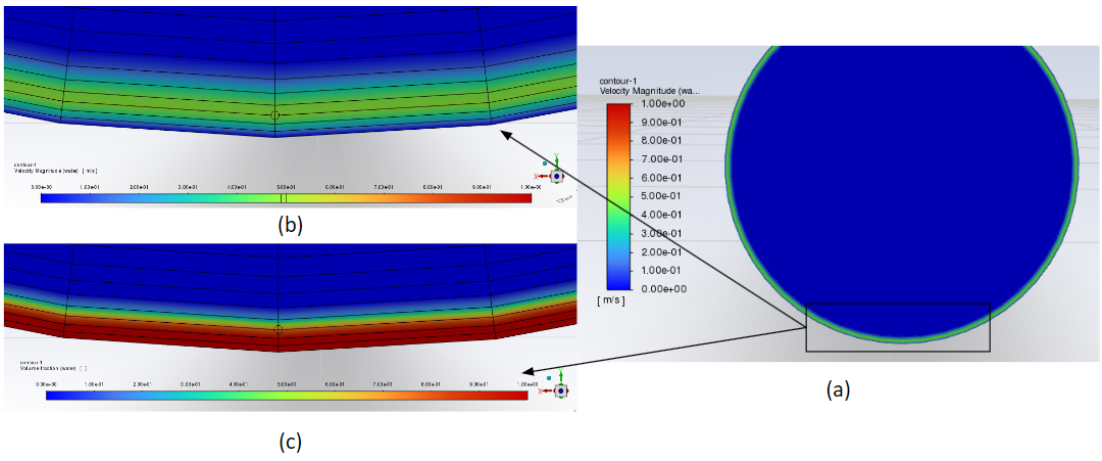

Figure 5.6: (a) and (b); Contour plot of the mixture velocity field in range 0-1 m/s at the outlet cross-section; (c); Water volume fraction at same place

In order to avoid the bubble size restriction associated with the Mixture model, the VoF method can be employed. It will allow for a broader range of Stokes numbers.

The non-physically low temperature in the inlet flow region can be avoided by defining a linear heat flux that increases downstream of the tube, but this is not an appreciated solution to the problem as it decreases linearly downstream of the tube, according to the experimental data. Moreover, the heat flux through the tube wall should be part of the solution, not a boundary condition. Therefore, all part of the geometry is included in the next attempt.

5.2.3 Configuration 3

The Lee coefficient (*coeff*) is gradually increased in this configuration. Again, the simulation becomes unstable when the *coeff* reaches higher values. Figure 5.7 shows the temperature profile (a) and the velocity profile (b) at the middle and outlet cross-lines in the steam domain just before the simulation becomes unstable (when the value of *coeff* is reached 22). As seen, there is a drop in both temperatures due to heat conduction through the tube wall and mixture velocity as more steam is condensed into water. At the point when this happens, the thickness of the condensed water film at the inner surface of the tube is not more than 0.2 mm (see Figure 5.9 (a)-(c)). Figure 5.8 (b) shows the velocity profile at the middle and outlet cross-line of the steam domain. It is visible how it starts to look close to the wall when the *coeff*-value is increased further to a value of 24. This is also visible in Figures 5.9 (b). Figure 5.10 (a) shows the Iso-clipped static temperature field below the saturation temperature, and Figure 5.10 (b) shows a nonzero mass transfer rate. Correlating 5.10 (a) with (b) indicates that condensation occurs in those regions where $T_i < T_{sat}$, however in Figure 5.10 (c) it can be seen that the volume fraction of water in the region is almost zero showing the massive deviation between the saturation and the interfacial temperature.

It's worth to note that the mesh in configuration 3 is finer than that in configuration 1, which has an influence on the *coeff* value. In configuration 1, mass and energy conservation are met when the *coeff* value reaches 70, whereas in configuration 3, these conservation criteria are satisfied at a *coeff* value of 22.

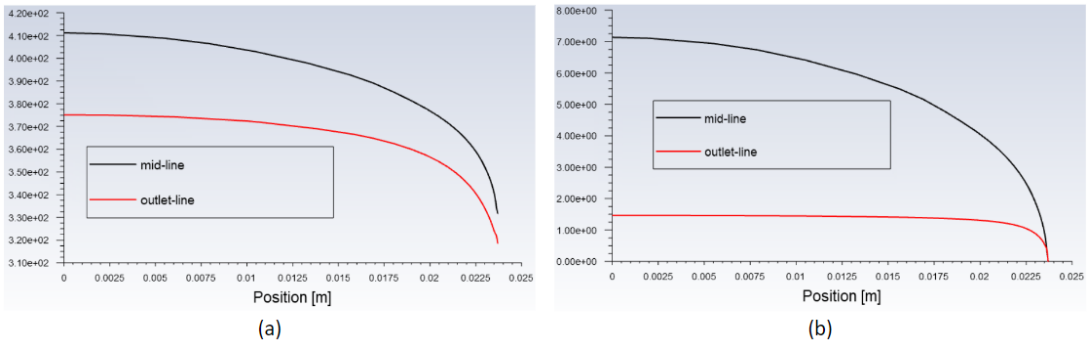

Figure 5.7: (a); Temperature profile at the middle (black) and outlet (red) cross-line of the steam domain, (b); Velocity profile at the middle (black) and outlet (red) cross-line of the steam domain, *coeff* = 22, (Temperature in Kelvin [K], Velocity in [m/s], Wall and center-line is located to right and left of the figures respectively)

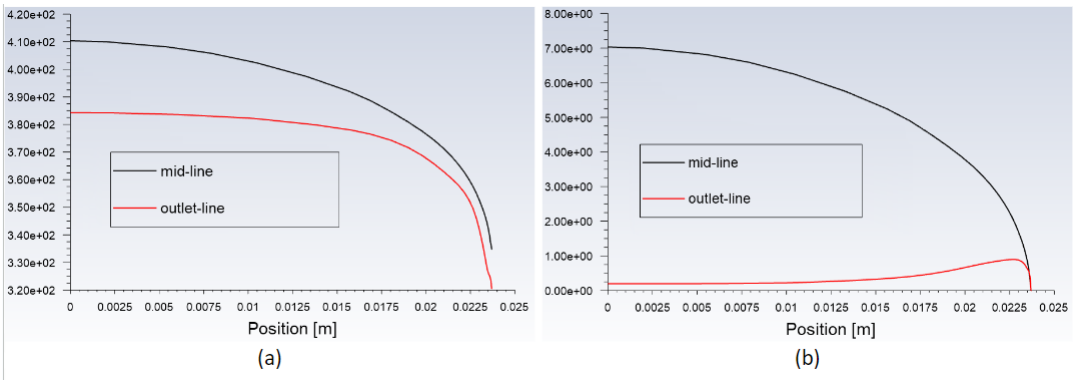

Figure 5.8: (a); Temperature profile at the middle (black) and outlet (red) of the steam domain, (b); Velocity profile at the middle (black) and outlet (red) of the steam domain, *coeff* = 24, (Temperature in Kelvin [K], Velocity in [m/s], Wall and center-line is located to right and left side of the figures respectively)

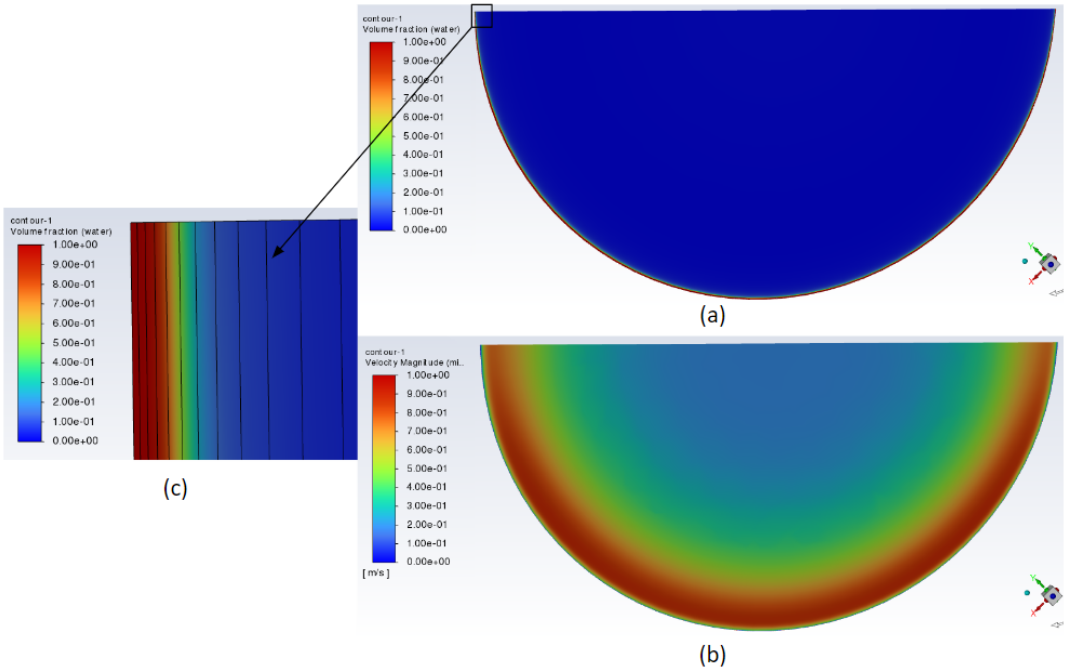

Figure 5.9: (a)-(c); Water volume fraction (red color indicates water and blue color strands for steam), (b); Velocity magnitude in range 0-1 [m/s] at the outlet of steam domain ,$coeff = 24$

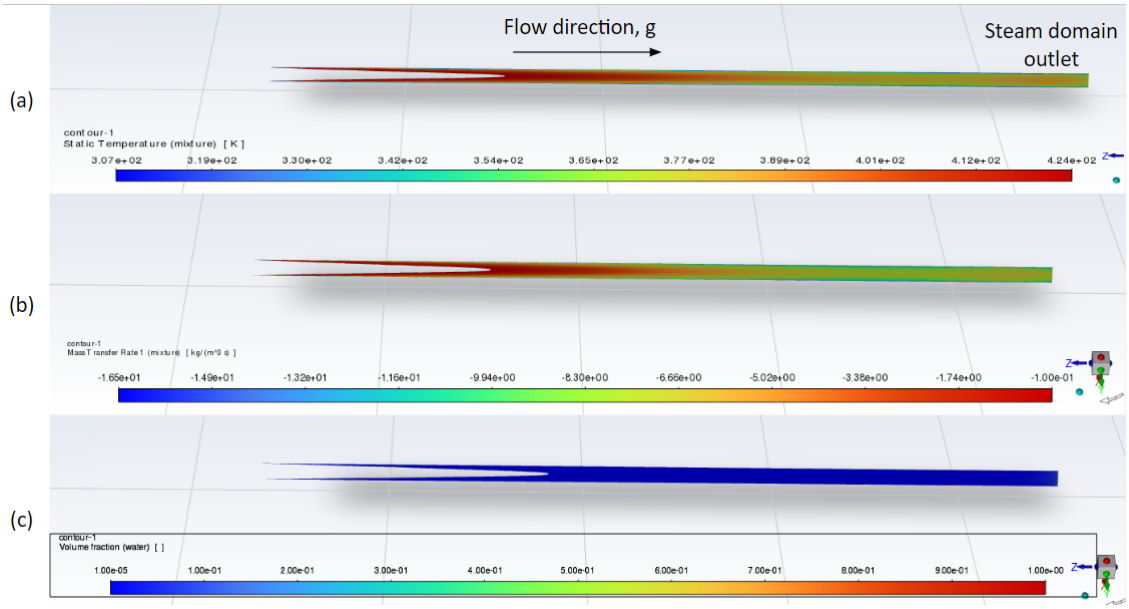

Figure 5.10: (a); Contour plot of temperature below the saturation temperature, (b); Contour plot of nonzero mass transfer rate, (c); Contour plot of water volume fraction in range 0.001 to 100 % (water is marked as red and steam is marked as blue)

6
Conclusion

6.1 Pipe Flow Case

The pipe flow case aims to learn about mesh requirements and fundamental settings to be used later. Lists below are the general conclusions from this case:

- It was found that quantities such as y^+ of the first cell away from the wall and the number of prism layers significantly affect the CFD results. Therefore, it is recommended to conduct a mesh convergence study
- In order to obtain a fully developed pipe flow, it is recommended to use a periodic boundary condition and a predefined turbulent characteristic velocity profile
- In order to ensure convergence, it is essential to monitor additional variables, such as wall shear stress, alongside the residuals criteria
- The results obtained from the simulation show a good correlation with the corresponding analytical solution with a maximum deviation of 1.5 % of wall shear stress and pressure drop

6.2 Kuhn Test Case

The current work mainly provides a baseline for the simulation of full condensation of water vapor in a vertical downflow circular tube using Ansys/Fluent. The key outcomes from the study are as follows:

- The mass transfer intensity (*coeff*) in the Lee condensation model greatly depends on the mesh size. The finer the mesh, the more sensitive it is.
- The significant deviation between T_{sat} and T_i (saturation- and interfacial temperature) implies the poor performance of the Lee condensation model
- Although the Mixture model gives insight into condensation, it relies on the flow Stokes number. Therefore, there are better models in the simulation of condensation. The VoF method provides a better foundation for this
- Despite the thickness of the condensate water film being very close to that of previous literature, simulation in the current work is not capturing full condensation as reported in the experiment.
- In order to obtain full condensation, more investigations need to be carried out in the future.

6.3 Future Work

The results presented in this project concern modeling of the experimental case *RUN 1.1-5R1* performed by Kuhn where full condensation occurs.

When dealing with multiphase flow modeling, including phase change (condensation), there are many factors and parameters that affect the simulation. Ranging from the choice of the multiphase model to the choice of the condensation model. However, some recommendations for the future work are formalized here;

- **Multiphase model**: Due to the limited time frame of this project, the full Eulerian multiphase model has not been adopted where other physical aspects can be taken into account which could have a significant effect on the simulation results
- **Condensation model**: To avoid tuning the coefficient (*coeff*) in the Lee model, it is highly recommended to use another condensation model that depends only on physical parameters, such as the temperature gradient.
- **Mesh**: The study did not analyze the effects of using different mesh types (i.e., Tetrahedral or Hexcore). Therefore, it may be valuable to explore other grid type instead of Polyhedral, as it could produce different results.
- **Experimental test case**: To see the effects of other forces besides gravity, it is recommended to find other experimental data with a smaller test section compared to the Kuhn test case.

Bibliography

[1] Tanrikut A. and O. Yesin. "In-Tube Steam Condensation in the Presence of Air". In: *Office of Nuclear Regulator Research, U.S. Nuclear Regulator Commision* (2007).

[2] Walter Ambrosini et al. "Experiments and modelling techniques for heat and mass transfer in light water reactors". In: *Science and Technology of Nuclear Installations* 2009 (2009), pp. 1–11.

[3] Bengt Andersson et al. "Multiphase flow modelling". In: Cambridge University Press, 2011, pp. 143–173.

[4] Bengt Andersson et al. "Multiphase flow modelling". In: *Computational Fluid Dynamics for Engineers*. Cambridge University Press, 2011, pp. 143–173. DOI: 10.1017/CBO9781139093590.007.

[5] *Ansys® Fluent*. Version 2023 R1. URL: https://www.ansys.com/products/fluids/ansys-fluent.

[6] *Ansys® Fluent Theory Guide*. Version 2023 R3, January 2023.

[7] *Ansys® Fluent User Guide*. Version 2023 R1, January 2023.

[8] Christopher E. Brennen. "Frontmatter". In: *Fundamentals of Multiphase Flow*. Cambridge University Press, 2005.

[9] Lars Davidson. *Fluid mechanics, turbulent flow and turbulence modeling*. Elsevier, 2023.

[10] P. Durbin. "Turbulent Flows. By S. B. POPE. Cambridge University Press, 2000. 771 pp. ISBN 0 521 59886 9. £29.95 or 49.95(*paperback*); $ISBN 0521591252. £80.00 or 130.0$ (hardback)." In: *Journal of Fluid Mechanics* 427 (2001), pp. 410–411. DOI: 10.1017/S0022112000212913.

[11] H.A. Hasanein, M.S. Kazimi, and M.W. Golay. "Forced convection in-tube steam condensation in the presence of noncondensable gases". In: *International Journal of Heat and Mass Transfer* 39.13 (1996), pp. 2625–2639. ISSN: 0017-9310. DOI: https://doi.org/10.1016/0017-9310(95)00373-8. URL: https://www.sciencedirect.com/science/article/pii/0017931095003738.

[12] S. Z. Kuhn, Virgil E. Schrock, and Per F. Peterson. "An investigation of condensation from steam–gas mixtures flowing downward inside a vertical tube". In: *Nuclear Engineering and Design* 177 (1997), pp. 53–69. URL: https://api.semanticscholar.org/CorpusID:109648094.

[13] Alfa Laval. *Brazed plate heat exchangers*. Tech. rep. URL: https://www.alfalaval.com/globalassets/documents/industries/refrigeration/brazed-plate-heat-exchangers.pdf.

[14] Alfa Laval. *The theory behind heat transfer*. Tech. rep. URL: https://www.alfalaval.com/globalassets/documents/microsites/heating-and-

cooling-hub/alfa_laval_heating_and_cooling_hub_the_theory_behind_heat_transfer.pdf.

[15] Hyoungsoon Lee et al. "Experimental and computational investigation of vertical downflow condensation". In: *International Journal of Heat and Mass Transfer* 85 (2015), pp. 865–879. ISSN: 0017-9310. DOI: https://doi.org/10.1016/j.ijheatmasstransfer.2015.02.037. URL: https://www.sciencedirect.com/science/article/pii/S0017931015002008.

[16] Hyoungsoon Lee et al. "Experimental and computational investigation of vertical downflow condensation". In: *International Journal of Heat and Mass Transfer* 85 (2015), pp. 865–879. ISSN: 0017-9310. DOI: https://doi.org/10.1016/j.ijheatmasstransfer.2015.02.037. URL: https://www.sciencedirect.com/science/article/pii/S0017931015002008.

[17] Hyoungsoon Lee et al. "Experimental and computational investigation of vertical downflow condensation". In: *International Journal of Heat and Mass Transfer* 85 (2015), pp. 865–879. ISSN: 0017-9310. DOI: https://doi.org/10.1016/j.ijheatmasstransfer.2015.02.037. URL: https://www.sciencedirect.com/science/article/pii/S0017931015002008.

[18] N Padoin and C Soares. "CFD modeling of steam condensation in industrial pipes". In: *Blucher Chemical Engineering Proceedings* 1.2 (2015), pp. 12904–12911.

[19] David Reay, Colin Ramshaw, and Adam Harvey. "Chapter 4 - Compact and Micro-heat Exchangers". In: *Process Intensification (Second Edition)*. Ed. by David Reay, Colin Ramshaw, and Adam Harvey. Second Edition. Isotopes in Organic Chemistry. Oxford: Butterworth-Heinemann, 2013, pp. 91–120. ISBN: 978-0-08-098304-2. DOI: https://doi.org/10.1016/B978-0-08-098304-2.00004-3. URL: https://www.sciencedirect.com/science/article/pii/B9780080983042000043.

[20] S.B. Al-Shammari, D.R. Webb, and P. Heggs. "Condensation of steam with and without the presence of non-condensable gases in a vertical tube". In: *Desalination* 169.2 (2004), pp. 151–160. ISSN: 0011-9164. DOI: https://doi.org/10.1016/j.desal.2003.11.006. URL: https://www.sciencedirect.com/science/article/pii/S0011916404005223.

[21] Mansoor Siddique, Michael W. Golay, and Mujid S. Kazimi. "Local Heat Transfer Coefficients for Forced-Convection Condensation of Steam in a Vertical Tube in the Presence of a Noncondensable Gas". In: *Nuclear Technology* 102.3 (1993), pp. 386–402. DOI: 10.13182/NT93-A17037. eprint: https://doi.org/10.13182/NT93-A17037. URL: https://doi.org/10.13182/NT93-A17037.

[22] National Institute of Standards and Technology. *NIST Chemistry WebBook*. Tech. rep. Washington, D.C.: U.S. Department of Commerce, 2023. DOI: https://doi.org/10.18434/T4D303.

[23] R. Szijártó et al. "Condensation models for the water–steam interface and the volume of fluid method". In: *International Journal of Multiphase Flow* 93 (2017), pp. 63–70. ISSN: 0301-9322. DOI: https://doi.org/10.1016/j.ijmultiphaseflow.2017.04.002. URL: https://www.sciencedirect.com/science/article/pii/S0301932216304530.

[24] Didi Zhang et al. “Simulation and experimental studies of R134a flow condensation characteristics in a pump-assisted separate heat pipe”. In: *International Journal of Heat and Mass Transfer* 126 (2018), pp. 1020–1030. ISSN: 0017-9310. DOI: https://doi.org/10.1016/j.ijheatmasstransfer.2018.06.057. URL: https://www.sciencedirect.com/science/article/pii/S001793101830526X.

DEPARTMENT OF SOME SUBJECT OR TECHNOLOGY
CHALMERS UNIVERSITY OF TECHNOLOGY
Gothenburg, Sweden
www.chalmers.se

CHALMERS
UNIVERSITY OF TECHNOLOGY